Article

Scattering of CO from Vacant-MoSe$_2$ with O Adsorbates: Is CO$_2$ Formed?

Published as part of The Journal of Physical Chemistry C special issue "Alec Wodtke Festschrift".

Raúl Bombín,* Ricardo Díez Muiño,* J. Iñaki Juaristi,* and Maite Alducin*

Read Online

ACCESS | 📊 Metrics & More | 📰 Article Recommendations | 🆂🅸 Supporting Information

ABSTRACT: Using ab initio molecular dynamics (AIMD) simulations, based on density functional theory that also accounts for van der Waals interactions, we study the oxidation of gas-phase CO on MoSe$_2$ with a Se vacancy and oxygen coverage of 0.125 ML. In the equilibrium configuration, one of the O atoms is adsorbed on the vacancy and the other one atop one Se atom. Recombination of the CO molecule with the second of these O atoms to form CO$_2$ is a highly exothermic reaction, with an energy gain of around 3 eV. The likeliness of the CO oxidation reaction on this surface is next examined by calculating hundreds of AIMD trajectories for incidence energies that suffice to overcome the energy barriers in the entrance channel of the CO oxidative recombination. In spite of this, no CO$_2$ formation event is obtained. In most of the calculated trajectories, the incoming CO molecule is directly reflected, and in some cases, mainly at low energies, the molecules remain trapped at the surface but without reacting. As an important conclusion, our AIMD simulations show that the recombination of CO molecules with adsorbed O atoms is a very unlikely reaction in this system, despite its large exothermicity.
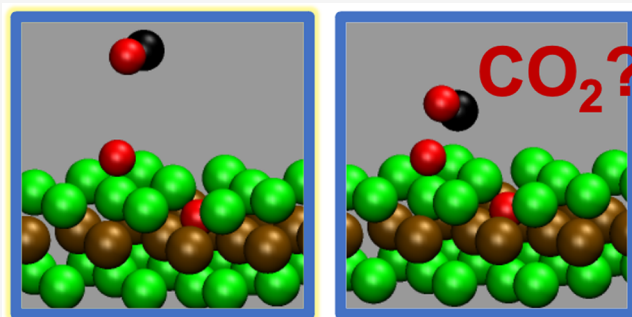
■ INTRODUCTION

In the last years, the possibility of using two-dimensional (2D) materials for catalysis[1−6] and gas sensing[7−10] has been broadly explored. Different families of 2D materials, like transition metal carbides or nitrides[11] and transition metal dichalcogenides (TMD),[12−18] have been considered for these purposes. The motivation roots in the exceptional properties that these materials exhibit for such applications, as for example, a large surface to volume ratio and good electronic and optical properties. Importantly, their properties can be tuned by several procedures, including application of strain,[19] application of an external electric field,[20] creation of vacancies,[21−25] stacking different two-dimensional materials,[10,26] and even by considering non 2D configurations.[27−29] The latter permits to engineer new 2D materials with the desired properties. For gas sensing and electrocatalysis applications, TMD semiconductors, in which we focus on in this work, offer the advantage of being easily implemented with electrodes,[16] while overcoming the zero band gap problem of graphene that complicates its implementation in electronic circuits.[30]

Focusing on the usage of TMDs as catalysts for diverse chemical processes, their applicability is promising. There are various studies exploring the catalytic properties of TMDs for the hydrogen evolution reaction (HER)[3,24,25,31−34] and the oxygen evolution reaction (OER).[35−37] These are the two reactions involved in water splitting, a key process for sustainable energy production. In the case of HER, TMD materials appear as good alternatives to precious metals such as platinum. However, pristine TMDs exhibit poor performance for OER due to the large binding energies of intermediate products on the TMD surface.[35] Nonetheless, both theory and experiments reveal that the efficiency of these two reactions can be enhanced at the edges of the nanosheets,[3,36,37] around chalcogen and metal vacancies,[24,31,32] and by doping the nanosheet.[33] Other chemical reactions that are the focus on theoretical studies of the TMD catalytic properties include, for example, CO$_2$ reduction to produce acids and other valuable products,[1,2,6,38−43] N$_2$ reduction to produce ammonia,[44] production of ethanol from syngas,[45] and also CO oxidation on MoS$_2$ doped with metal atoms,[46,47] on PtTe$_2$ in the presence of O$_2$,[48] and on the Janus WSSe surface.[49]
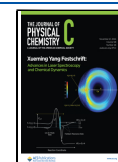
In the aforereviewed bibliography, the catalytic properties are commonly determined in terms of the adsorption energies and minimum energy paths of the reaction considered. Being the

latter the common procedure, the purpose and novelty of our work are to explore the catalytic properties of $MoSe_2$ for CO_2 formation but from a different perspective, the reaction dynamics. DFT calculations including van der Waals corrections showed that the dissociative adsorption of O_2, which is endothermic by more than 1 eV in the pristine $1H$-$MoSe_2$ sheet, becomes highly exothermic in the presence of Se vacancies.[50] In light of those results, here we focus on the dynamics of the recombination process between one O atom adsorbed on the $MoSe_2$ surface with a Se vacancy and a gas-phase CO molecule. This kind of reaction process, which can occur upon a single collision of the gas species with either the adsorbate (direct Eley−Rideal) or the surface (indirect Eley−Rideal) or after few collisions that serve to slow down the incoming atom/molecule (hot atom/molecule abstraction), are expected to efficiently compete with the thermal Langmuir−Hinshelwood recombination when the adsorbate is strongly bound to the surface. This is precisely the case in the dissociative adsorption of O_2 on the $MoSe_2$ surface with a Se vacancy. As shown in ref 50, the adsorption energies of the nascent O atoms formed upon the dissociative adsorption of O_2 in that surface are as strong as −2.9 and −7.3 eV, depending on the adsorption site. Our new calculations for the recombinative formation of CO_2 via an Eley−Rideal mechanism show that the reaction is energetically favored and thus, motivated us to study the process with ab initio molecular dynamics simulations (AIMD). Interestingly, none of the incoming CO molecules is able to abstract an O adatom and form CO_2, even if the molecule has enough energy to overcome the entrance barriers for the reaction. These results remark the importance of going beyond static calculations of the reaction energetics in determining the catalyzing character of the material under consideration.

The paper is organized as follows, the general computational settings employed to both model the system and simulate the reaction dynamics with the AIMD methodology are detailed in the Theoretical Methods section. The Results and Discussion section starts with the analysis of the energetics of the main reactions that may occur in the system for the incidence conditions considered, i.e., a gas-phase CO impinging on the $MoSe_2$ surface with a Se vacancy and an oxygen coverage of 0.125 ML. Next, the AIMD results are presented and discussed in light of the information extracted from the in depth analysis of the trajectories. The summary and Conclusions of our work are given in the last section.

THEORETICAL METHODS

General DFT Computational Settings. All DFT calculations are performed with the Vienna ab initio simulation package (VASP)[51] using the revPBE-vdW exchange-correlation functional proposed by Dion et al.[52] The ionic cores are described with the projector augmented wave (PAW) method[53] implemented in VASP.[54] Specifically, we use the PAW potentials for Mo, Se, O, and C that have 14, 6, 6, and 4 valence electrons, respectively. The Kohn−Sham states are expanded in a plane-wave basis set using an energy cutoff of 700 eV. The Brillouin zone integration is performed with a Γ-centered $4 \times 4 \times 1$ Monkhorst−Pack grid of special **k**-points.[55] A Gaussian smearing of 0.1 eV is used for electronic state occupancies.

Calculations are performed for the $1H$ phase of the $MoSe_2$ monolayer with a small concentration of noninteracting Se vacancies (denoted as $MoSe_2$-vSe hereafter). Following ref 50, the latter is adequately described by a 4×4 surface supercell that contains a single Se vacancy and is separated from its periodic

image by 23 Å of vacuum along the surface normal. The value of the hexagonal lattice constant is $a = 3.386$ Å.[50] The O_2 molecule is dissociatively adsorbed in the configuration analyzed in ref 50. Namely, one of the O atoms is adsorbed on top of the Se vacancy and the other one on top of the closest Se atom. The O atom in the vacancy is located at $z = -0.62$ Å below the surface, the O atom on top of the Se atom is located at $z = 1.57$ Å above the surface, and the distance between them is d(O−O) = 4.01 Å. Dissociation of the O_2 molecule in this configuration is exothermic by 3.3 eV. We denote this structure as 2O-$MoSe_2$-vSe.

Regarding our choice of the revPBE-vdW functional, our previous study of the adsorption properties of different diatomic molecules on $MoSe_2$ and $MoSe_2$-vSe showed that both revPBE-vdW and PBE-D3[56] provide a satisfactory description of the experimental $MoSe_2$ geometrical and electronic structures. Furthermore, even if PBE-D3 tends to overbinding as compared to revPBE-vdW, there were no significant qualitative differences between both functionals in the O, O_2, and CO adsorption and dissociation energies and adsorption sites on $MoSe_2$ and $MoSe_2$-vSe.

AIMD Initial Conditions. The interaction dynamics of CO with the 2O-$MoSe_2$-vSe surface is studied with total energy-conserving AIMD simulations for an initial substrate temperature of 100 K. The initial positions and velocities of the atoms in the substrate are randomly taken from a canonical ensemble of configurations. The latter is generated by thermalizing the 2O-$MoSe_2$-vSe substrate at 100 K during more than 10 ps using the Nosé−Hoover thermostat[57] implemented in VASP. The use of constant-energy AIMD simulations with an appropriate set of initial positions and velocities constitutes a reasonable approximation to incorporate surface temperature effects during the short simulation time of interest (up to 1.0−1.4 ps in our case).[58] This is a common procedure in gas-surface dynamics simulations.[58−68]

The CO molecule starts with its center of mass (CM) located at a distance $Z_{cm} = 6$ Å from the 2O-$MoSe_2$-vSe surface with the vibrational zero-point energy and zero rotational energy. The initial molecular orientation and CM position in the (x, y)-plane parallel to the surface are randomly sampled. The (X_{cm}, Y_{cm})-sampling however focuses on the simulation cell area that contains the O adatoms with the purpose of optimizing the computational effort (see below). The molecule impinges perpendicular to the surface (i.e., normal incidence). Simulations are performed for five different initial translational energies, namely, $E_i = 0.2, 0.4, 0.6, 0.8,$ and 1.0 eV. For each E_i, 200 AIMD trajectories are run using the Beeman predictor-corrector algorithm with an integration time step of 1 fs. At the end of each AIMD trajectory, the impinging CO is considered reflected when its center of mass reaches a distance from the Se topmost layer $Z_{cm} \geq 6$ Å with positive velocity along the surface normal ($P_{cm,z} > 0$). It is considered trapped if after reaching the maximum integration time of 1 ps, the previous condition was not met. In the case of recombinative CO_2 formation, the same criteria is used to distinguish between CO_2 desorption and trapping.

RESULTS AND DISCUSSION

The calculated reaction energies summarized in Table 1 show that both the recombinative CO_2 adsorption (−3.437 eV) and abstraction (−3.174 eV) involving the O atom adsorbed atop Se (O_{top} hereafter) are highly exothermic. Recombination with the O atom adsorbed in the Se vacancy (O_{vac} hereafter) is

Table 1. Reaction Energies E for $CO_{(g)} + O_{(a)}$ Recombinative Abstraction, $CO_{(g)} + O_{(a)}$ Recombinative Adsorption, and $CO_{(g)}$ Adsorption on the 2O-MoSe$_2$-vSe Surface[a]

reaction	reactant/product adsorption site	E (eV)
$CO_{(g)} + O_{(a)} \rightarrow CO_{2(g)}$	$O_{top}/-$	−3.174
$CO_{(g)} + O_{(a)} \rightarrow CO_{2(g)}$	$O_{vac}/-$	1.297
$CO_{(g)} + O_{(a)} \rightarrow CO_{2(a)}$	$O_{top}/CO_2\,O_{vac}$	−3.437
$CO_{(g)} + O_{(a)} \rightarrow CO_{2(a)}$	$O_{vac}/CO_2\,O_{vac}$	−0.286
$CO_{(g)} \rightarrow CO_{(a)}$	$-/CO_h$	−0.154

[a]Corresponding reactant/product adsorption sites are also indicated. The subscripts (g) and (a) stand for "gas" and "adsorbed", respectively.

energetically less favored. In particular, adsorption is exothermic by only −0.286 eV, while abstraction becomes endothermic, being the reaction energy 1.297 eV. The different adsorption energy for O_{top} (−2.872 eV) and O_{vac} (−7.300 eV)[50] is the main reason for the different reaction energies obtained with each adsorbate. CO adsorption near O_{top} although exothermic is energetically less favored than CO_2 formation. In this adsorption configuration (denoted as CO_h in Table 1), the CO center of mass is practically over a hollow site (see the black-framed panel in Figure 1). Interestingly, the calculated CO_h adsorption energy
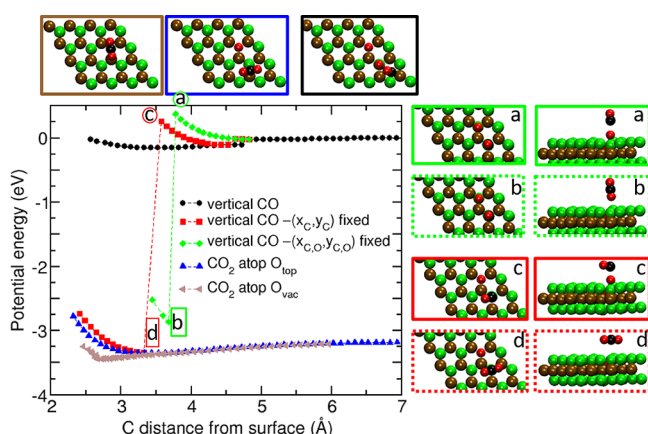

Figure 1. Potential energy against the C distance from the topmost Se layer z_C. The zero reference energy corresponds to CO in the middle of vacuum. Black, red, and green curves correspond to a vertically oriented CO approaching the surface above O_{top} under different relaxation conditions (see text for details). Brown and blue curves correspond, respectively, to the CO + O_{top}-recombined CO_2 approaching the surface over O_{vac} and over the Se atom on which O_{top} was adsorbed. The three structures on the top and from left to right correspond to the minimum energy configurations for the curves labeled CO_2 atop O_{vac} (brown curve), CO_2 atop O_{top} (blue curve), and vertical CO (black curve). Top and side views of the structures before and after the discontinuities in the red (points labeled c and d) and green (points labeled a and b) vertical CO curves are shown in the right panels following the same labeling. Se (top layer), Mo, O, and C are plotted in green, brown, red, and black, respectively.

on 2O-MoSe$_2$-vSe (−0.154 eV) is similar to that of CO adsorbed over a hollow site on pristine MoSe$_2$ (−0.143 eV).[50] Nonetheless, since the focus of this work is the recombinative formation of CO_2, we did not perform a systematic analysis of all possible CO adsorption configurations on 2O-MoSe$_2$-vSe and, therefore, we cannot discard the existence of CO adsorption configurations more stable than CO_h.

In addition to calculating the reaction energy, we carried out a preliminary inspection of the possible energy barriers the incoming CO may encounter while approaching the surface. For simplicity, we focused on exploring a few paths running close to O_{top}. In these calculations the height of the C atom z_C (and the 3 coordinates of one Mo atom located more than 7 Å away the O adsorbates) are always fixed. In some paths, also the (x, y) coordinates of the C and O atoms forming the molecule are fixed. The rest of degrees of freedom are allowed to relax until forces are smaller than 0.015 eV/Å. The dependence of the potential energy on z_C along these inspection paths is represented in Figure 1. A vertically oriented CO approaching atop O_{top} will face an energy barrier of about 0.378 eV, if the CO molecule is forced to stay perpendicular to O_{top} by fixing the center of mass coordinates (X_{cm}, Y_{cm}) (green diamonds). The abrupt energy decrease at $z_C \simeq 3.5$ Å corresponds to abstraction of the adsorbed O to form a vertically oriented CO_2 (see top and side views of the structures at points a and b in Figure 1). Note that the energy at b is greater than that of desorbed CO_2 (asymptotic limit of the CO_2 curves plotted by blue and brown triangles in the figure), suggesting that an eventually formed vertical-CO_2 will end desorbing. The latter was confirmed with an ulterior structural relaxation of the system configuration at b, which ends with the CO_2 molecule in vacuum. A similar energy barrier (0.260 eV) is found when only the C coordinates (x_C, y_C, z_C) are fixed (red squares). In this case CO can tilt while approaching O_{top} (see structure c in Figure 1) and also ends forming CO_2 (see structure d), giving rise to the energy drop observed between points c and d in the figure. In this case the formed molecule is oriented parallel to the surface and it is energetically more stable than the desorbed CO_2. Finally, when only z_C is fixed while approaching over O_{top}, CO tilts and is progressively repealed away the initial $O_{top}-C$ vertical line, avoiding the energy barriers found in the two previous paths. The minimum energy configuration along this path is shown in the black framed panel. For completeness, we also calculate potential energy curves against z_C for the CO_2 formed from $CO_{(g)} + O_{top}$. In these calculations only z_C is fixed. Energies for CO_2 approaching over O_{vac} and atop the Se atom on which O_{top} was adsorbed prior recombining are respectively plotted by brown and blue curves in Figure 1. Corresponding minimum energy structures are depicted in the brown and blue framed panels.

Although CO_2 formation and desorption upon O_{top} abstraction is energetically favored, the previous analysis casts some doubts regarding the likeliness of the reaction. The explored paths present energy barriers in the entrance channel that may difficult the required approach of the CO molecule to O_{top} prior recombining. Nevertheless, we cannot exclude the existence of other complex but more favorable reaction paths with lower or nonexistent energy barriers. In this respect, there are many examples showing that the incoming gaseous species can also capture the adsorbate upon reflecting once (indirect ER recombination) or several times (hot atom/molecule recombination) with the surface. Both direct and indirect ER recombination are observed in molecular dynamics (MD) and AIMD simulations of $H_{(g)}$ scattered off Cl/Au(111)[69,70] and H/Cu(111)[71,72] and in MD simulations of $N_{(g)}$ scattered off N-covered Ag(111)[73,74] and N-covered W(110),[75−77] whereas only indirect ER occurs in the N-covered W(100)[75,76] even at grazing incidence conditions at which direct ER is likely to occur[77] and, important for the present study, in the formation of CO_2 by $O_{(g)}$ atoms impinging on CO/Pt(111).[78] In the case of

$H_{(g)}$ impinging on H-covered W(110) and W(100) surfaces, all ER recombinations are indirect,[77] being also important the hot atom mechanism as shown in ulterior simulations performed at finite coverage.[79−81]

Considering the rich reactivity observed in other systems, the results of our AIMD calculations are quite surprising. Even if most of the simulated incidence energies (E_i = 0.2−1.0 eV) suffice to overcome the energy barriers explored in Figure 1, none of the trajectories led to CO_2 formation. The latter includes both desorption and trapping (adsorption) of the expected $CO_{(g)}$ + $O_{(a)}$ recombination. There are only two possible outcomes observed at the end of simulations that correspond to the impinging CO being either reflected or molecularly trapped on the surface. Processes such as $O_{(a)}$ atomic desorption or O_2 recombinative desorption are highly endothermic and, therefore, energetically forbidden for the incidence energies here considered. Figure 2 shows the
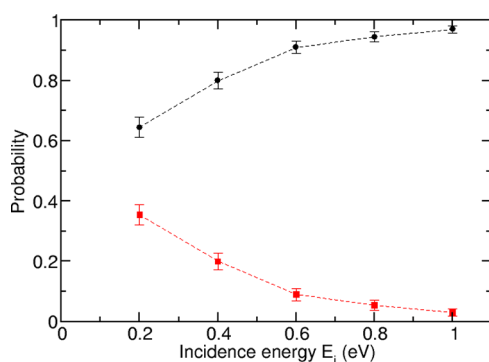

Figure 2. Scattering (black circles) and trapping (red squares) probability against incidence energy E_i for CO impinging normal to the 2O-MoSe$_2$-vSe surface.

probabilities for CO reflection and trapping as a function of the incidence energy E_i. At the lowest considered energy (E_i = 0.2 eV) 65% of the molecules are reflected, whereas a high 35% of them remain dynamically trapped at the end of the simulations (1 ps). Once the first collision with the surface takes place within a short interval of 200−400 fs, the trapped CO molecules experience a second rebound in the vacuum side at very diverse heights (3.5 ≤ Z_{cm} < 6 Å) and are attracted back to the surface. After extending the integration time up to about 1.4 ps, all these molecules stay below 6 Å from the surface, but the final outcome of these trajectories at longer times remains unclear with our limited-time dynamics (see Figure S1 in the Supporting Information). As E_i increases, the trapping probability rapidly decreases in favor of CO reflection. Thus, at the largest E_i = 1 eV more than 95% of the molecules are reflected. With very few exceptions, observed at lower incidence energies, the reflection process occurs after the very first collision with the surface. For E_i = 0.2, 0.4 eV, the first (classical) turning point of the reflected molecules is distributed in three regions depending on whether CO collides near O_{top} (Z_{cm} ≥ 3.5 Å), near O_{vac} (Z_{cm} ≤ 2.25 Å), or at other points on the surface (2.25 < Z_{cm} < 3.5 Å). These turning point regions move closer to the surface and broaden as E_i increases. The turning point distributions for the trapped molecules exhibit a less featured structure. All these observations can be seen in Figures S2−S4 in the Supporting Information.

A more thorough analysis of the trajectories allows us to better understand the lack of recombination processes. Figures 3 and 4
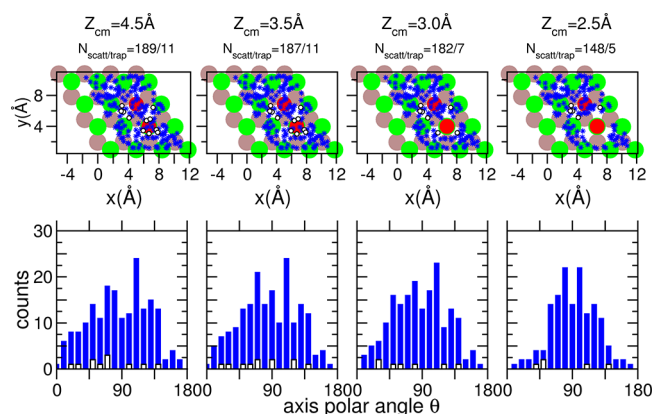

Figure 3. Evolution of the reflected (blue crosses and bars) and trapped (black empty circles and bars) CO molecules along the incoming trajectory impinging normal to 2O-MoSe$_2$-vSe with an initial incidence kinetic energy E_i = 0.4 eV. Top: CO center of mass position over the surface unit cell when first reaching the height Z_{cm} given above each column together with the number of reflected and trapped CO that reach that height. Bottom: polar angle distribution of CO molecular axis for a 10° binning. Se (top layer) and Mo surface atoms and O adatoms are represented by green, brown, and red circles, respectively.
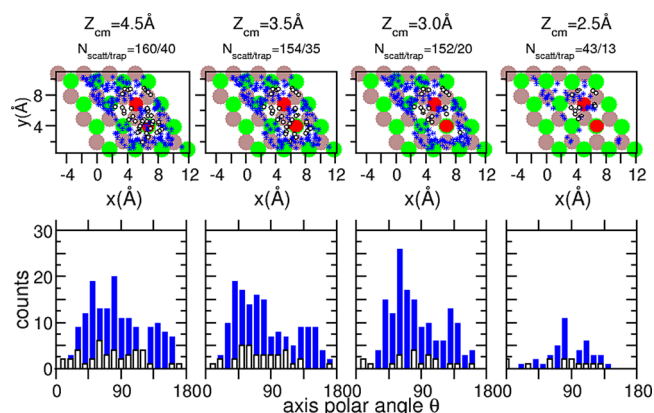

Figure 4. Same as Figure 3 but for initial incidence kinetic energy E_i = 0.8 eV.

show the evolution along the incoming trajectory of the CO center of mass coordinates (X_{cm}, Y_{cm}) and the polar angle w.r.t. the surface normal of the CO molecular axis θ for incidence energies E_i = 0.4 eV and E_i = 0.8 eV, respectively. (Note in passing that the center of mass position at Z_{cm} = 4.5 Å provides a clear idea of the area covered by the random distribution over the surface that was used in the initial conditions sampling described in sec AIMD Initial Conditions.) The number of reflected and trapped molecules that reach a certain height Z_{cm} during the initial approach is written on each column, providing information on how many molecules have experienced the first collision with the surface between two consecutive height values. The most salient feature in both figures is the inability of the CO molecules to get close enough to O_{top}. In the case of E_i = 0.4 eV, already at Z_{cm} = 3.5 Å, molecules that were impinging nearby O_{top} have been reflected (6 molecules) or have been deviated to remain trapped at the surface (5 molecules). At the higher energy E_i = 0.8 eV (Figure 4), the molecules can get closer. Yet two of the molecules incoming above O_{top} have already been reflected at Z_{cm} = 3.5 Å and at Z_{cm} = 3 Å all the molecules that were approaching O_{top} have been reflected or deviated from the

O_{top} proximity in the case of the trapped molecules. Interestingly, a majority of the molecules that can get as close to the surface as Z_{cm} = 2.5 Å are the ones that are in the region close to O_{vac}. However, O_{vac} is buried in the Se topmost layer $(-0.62$ Å$)^{[50]}$ and strongly bound to the substrate, such that recombination does not take place. Regarding the θ distributions, there is no noticeable effect related to the orientation of the molecules, except for a certain predominance of near parallel orientations $(45° < \theta < 135°)$ at the closest distances.

These results are consistent with the information obtained from the reaction paths analyzed in Figure 1. The reaction is highly exothermic and direct once the CO molecule is close to O_{top}, with the C atom at a distance from the surface below 3.5−4 Å depending on its orientation. However, the energy barriers that exist in the incoming path prevent the molecules from reaching that configuration. As a consequence, the CO molecules either reflect directly on top of O_{top} before getting close enough to react, or are deviated and remain trapped at the surface. Though we cannot completely exclude that the trapped molecules may eventually get close to the O_{top} in a proper orientation and react, the probability for this process is expected to be very low, considering that it has not occurred in any of the trapped trajectories for which the integration time has been increased up to 1.2−1.4 ps. In any case, in spite of its high exothermicity, direct ER recombination between CO impinging from vacuum and O_{top} can apparently be excluded. To further support this conclusion, one additional trajectory was run for each E_i, in which the initial CO coordinates correspond to a vertically oriented CO located exactly above O_{top} at height $Z_{cm} \simeq$ 4.5 Å. The turning point (taken as the height of the C atom) decreases to 2.49 Å for E_i = 0.2 eV and to 2.03 Å for E_i = 1.0 eV but in all cases the CO molecule bounces back into vacuum highly rotationally excited without forming a stable O_{top}−C bound.

Regarding the difference between reflected and trapped CO, Figures 3 and 4 suggest that those molecules initially impinging over or nearby O_{top} are more likely to be trapped after the first collision with the surface. But there is also a certain amount of trapped molecules that were initially located nearby O_{vac}. The evolution of the molecular orientation features no apparent differences between reflected and trapped CO. Altogether the difference between direct reflection and trapping seems related to minor details of the potential energy felt by the incoming CO molecule.

Finally, focusing on the reflected trajectories, in the left panel of Figure 5 we observe that these molecules are predominantly reflected with small outgoing angles ($<40°$). This is expected for

molecules under normal incidence that are directly reflected, i.e., without experiencing any relevant deviation along the incoming trajectory. The latter suggests a negligible corrugation of the potential energy surface as compared to the incidence energy E_i. In this respect, the wider distribution of the outgoing angle at E_i = 0.2 eV agrees with the early energy barriers discussed above. Upon colliding with the surface, the reflected molecules become quite rotationally excited, particularly for incidence energies E_i = 0.6, 0.8, and 1.0 eV. As shown in the right panel of Figure 5, the rotational quantum number reaches values as high as $J \geq 35$ for the largest studied E_i.

■ CONCLUSIONS

We have studied the interaction of CO molecules coming from vacuum and a 2O-MoSe$_2$-vSe surface, in which one O atom is adsorbed in a Se vacancy and a second O atom is adsorbed on top of a Se atom of the $1H$ phase of the MoSe$_2$ monolayer. The latter is the equilibrium structure upon (dissociative) adsorption of a O$_2$ molecule on a MoSe$_2$ monolayer with one Se vacancy.[50] Interestingly, DFT calculations show that the CO recombination with the O atom adsorbed on top of the Se atom with either subsequent adsorption or desorption of the formed CO$_2$ molecules are highly exothermic reactions with energy gains of around 3−3.5 eV. Motivated by this finding, we have performed AIMD simulations with five different initial translational energies of CO molecules scattered off a 2O-MoSe$_2$-vSe surface thermalized at 100 K. Our aim was to analyze how likely was the CO oxidation in this system and the corresponding reaction mechanisms. However, none of the 200 AIMD trajectories run for each energy has led to CO$_2$ formation. The majority of the CO molecules are directly reflected, albeit in some cases (mainly at the lowest analyzed energies) some of them remain trapped at the surface without reacting with the adsorbed O atoms. The analysis of the trajectories show that those CO molecules impinging on O_{top} are reflected or deviated to trapping before they can get close enough to the O atom in order recombination can occur. Inspection of the possible reaction paths suggests that the configurational space of the oxidation process via an Eley– Rideal process is very restrictive. Due to the unavoidable limited statistics and integration time, which does not allow to completely determine the final outcome of the trapped CO molecules, we can not absolutely exclude the possibility of the reaction to occur at a later stage. Nevertheless, we can safely conclude that, in spite of its large exothermicity, the recombinative CO$_{(g)}$ + O$_{(a)}$ abstraction is in the best case a very unlikely reaction in this system. As a general and important conclusion, the results of our dynamics simulations remark the importance of going beyond a pure static analysis of the reaction energetics to determine the catalytic character of any material.

■ ASSOCIATED CONTENT

ⓈI Supporting Information

The Supporting Information is available free of charge at https://pubs.acs.org/doi/10.1021/acs.jpcc.4c06306.

> Detailed information on the turning point for the reflected and trapped molecules (PDF)

■ AUTHOR INFORMATION

Corresponding Authors

Raúl Bombín − *Institut des Sciences Moléculaires (ISM), Université de Bordeaux, 33405 Talence, France;* ◉ orcid.org/ 0000-0002-4553-1214; Email: raul.bombin@u-bordeaux.fr
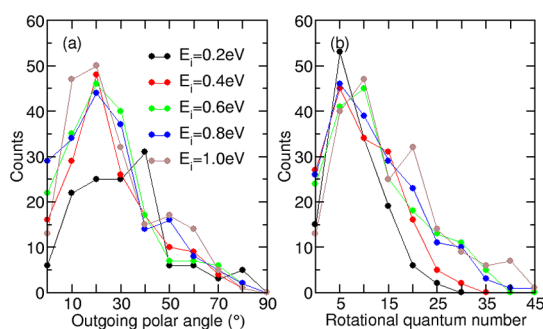
Figure 5. Outgoing polar angle (a) and rotational quantum number (b) distributions of the reflected CO molecules. Different colors correspond to different incidence energies E_i.

Ricardo Díez Muiño − *Donostia International Physics Center (DIPC), 20018 Donostia-San Sebastián, Spain; IKERBASQUE, Basque Foundation for Science, 48009 Bilbao, Spain;* ⓞ orcid.org/0000-0001-8593-0327; Email: rdm@ehu.eus

J. Iñaki Juaristi − *Departamento de Polímeros y Materiales Avanzados: Física Química y Tecnología, Facultad de Químicas (UPV/EHU), 20080 Donostia-San Sebastián, Spain; Centro de Física de Materiales CFM/MPC (CSIC-UPV/EHU), 20018 Donostia-San Sebastián, Spain; Donostia International Physics Center (DIPC), 20018 Donostia-San Sebastián, Spain;* ⓞ orcid.org/0000-0002-4208-8464; Email: josebainaki.juaristi@ehu.eus

Maite Alducin − *Centro de Física de Materiales CFM/MPC (CSIC-UPV/EHU), 20018 Donostia-San Sebastián, Spain; Donostia International Physics Center (DIPC), 20018 Donostia-San Sebastián, Spain;* ⓞ orcid.org/0000-0002-1264-7034; Email: maite.alducin@ehu.eus

Complete contact information is available at:
https://pubs.acs.org/10.1021/acs.jpcc.4c06306

Notes

The authors declare no competing financial interest.

■ REFERENCES

(1) Singh, S.; Modak, A.; Pant, K. K.; Sinhamahapatra, A.; Biswas, P. MoS₂−Nanosheets-Based Catalysts for Photocatalytic CO₂ Reduction: A Review. *ACS Appl. Nano Mater.* **2021**, *4*, 8644−8667.

(2) Giuffredi, G.; Asset, T.; Liu, Y.; Atanassov, P.; Di Fonzo, F. Transition Metal Chalcogenides as a Versatile and Tunable Platform for Catalytic CO₂ and N₂ Electroreduction. *ACS Mater. Au* **2021**, *1*, 6−36.

(3) Wazir, M. B.; Daud, M.; Safeer, S.; Almarzooqi, F.; Qurashi, A. Review on 2D Molybdenum Diselenide (MoSe₂) and Its Hybrids for Green Hydrogen (H₂) Generation Applications. *ACS Omega* **2022**, *7*, 16856−16865.

(4) Adabala, S.; Dutta, D. P. A Review on Recent Advances in Metal Chalcogenide-Based Photocatalysts for CO₂ Reduction. *J. Environ. Chem. Eng.* **2022**, *10*, No. 107763.

(5) Arumugam, M.; Yang, H.-H. A Review of the Application of Wide-Bandgap Semiconductor Photocatalysts for CO₂ Reduction. *J.CO2 Util.* **2024**, *83*, No. 102808.

(6) Khaidar, D. M.; Isahak, W. N. R. W.; Ramli, Z. A. C.; Ahmad, K. N. Transition Metal Dichalcogenides-Based Catalysts for CO₂ Conversion: An Updated Review. *Int. J. Hydrogen Energy* **2024**, *68*, 35−50.

(7) Tang, Y.; Zhao, Y.; Liu, H. Room-Temperature Semiconductor Gas Sensors: Challenges and Opportunities. *ACS Sens.* **2022**, *7*, 3582−3597.

(8) Tsai, H.-S.; Wang, Y.; Liu, C.; Wang, T.; Huo, M. The Elemental 2D Materials Beyond Graphene Potentially Used as Hazardous Gas Sensors for Environmental Protection. *J. Hazard. Mater.* **2022**, *423*, No. 127148.

(9) Sulleiro, M. V.; Dominguez-Alfaro, A.; Alegret, N.; Silvestri, A.; Gómez, I. J. 2D Materials Towards Sensing Technology: From Fundamentals to Applications. *Sens. Bio-Sens. Res.* **2022**, *38*, No. 100540.

(10) Ottaviano, L.; Mastrippolito, D. The Future Ahead Gas Sensing with Two-Dimensional Materials. *Appl. Phys. Lett.* **2023**, *123*, No. 050502.

(11) Sai Bhargava Reddy, M.; Aich, S. Recent Progress in Surface and Heterointerface Engineering of 2D MXenes for Gas Sensing Applications. *Coord. Chem. Rev.* **2024**, *500*, No. 215542.

(12) Liu, X.; Ma, T.; Pinna, N.; Zhang, J. Two-Dimensional Nanostructured Materials for Gas Sensing. *Adv. Funct. Mater.* **2017**, *27*, No. 1702168.

(13) Ping, J.; Fan, Z.; Sindoro, M.; Ying, Y.; Zhang, H. Recent Advances in Sensing Applications of Two-Dimensional Transition Metal Dichalcogenide Nanosheets and Their Composites. *Adv. Funct. Mater.* **2017**, *27*, No. 1605817.

(14) Zeng, Y.; Lin, S.; Gu, D.; Li, X. Two-Dimensional Nanomaterials for Gas Sensing Applications: The Role of Theoretical Calculations. *Nanomaterials* **2018**, *8*, 851.

(15) Vargas-Bernal, R. Electrical Properties of Two-Dimensional Materials Used in Gas Sensors. *Sensors* **2019**, *19*, 1295.

(16) Tyagi, D.; Wang, H.; Huang, W.; Hu, L.; Tang, Y.; Guo, Z.; Ouyang, Z.; Zhang, H. Recent Advances in Two-Dimensional-Material-Based Sensing Technology Toward Health and Environmental Monitoring Applications. *Nanoscale* **2020**, *12*, 3535−3559.

(17) Zheng, W.; Liu, X.; Xie, J.; Lu, G.; Zhang, J. Emerging van der Waals Junctions Based on TMDs Materials for Advanced Gas Sensors. *Coordin. Chem. Rev.* **2021**, *447*, No. 214151.

(18) Zhai, W.; Li, Z.; Wang, Y.; Zhai, L.; Yao, Y.; Li, S.; Wang, L.; Yang, H.; Chi, B.; Liang, J.; et al. Phase Engineering of Nanomaterials: Transition Metal Dichalcogenides. *Chem. Rev.* **2024**, *124*, 4479−4539.

(19) Muoi, D.; Hieu, N. N.; Phung, H. T.; Phuc, H. V.; Amin, B.; Hoi, B. D.; Hieu, N. V.; Nhan, L. C.; Nguyen, C. V.; Le, P. Electronic Properties of WS₂ and WSe₂ Monolayers with Biaxial Strain: A First-Principles Study. *Chem. Phys.* **2019**, *519*, 69−73.

(20) Ai, W.; Kou, L.; Hu, X.; Wang, Y.; Krasheninnikov, A. V.; Sun, L.; Shen, X. Enhanced Sensitivity of MoSe₂ Monolayer for Gas Adsorption Induced by Electric Field. *J. Phys-Condens. Mater.* **2019**, *31*, 445301.

(21) dos Santos, R. M.; da Cunha, W. F.; Giozza, W. F.; de Sousa Júnior, R. T.; Roncaratti, L. F.; Ribeiro Júnior, L. A. Electronic and Structural Properties of Janus MoSSe/MoX₂ (X = S,Se) in-plane Heterojunctions: A DFT Study. *Chem. Phys. Lett.* **2021**, *771*, No. 138495.

(22) Liang, Q.; Zhang, Q.; Zhao, X.; Liu, M.; Wee, A. T. S. Defect Engineering of Two-Dimensional Transition-Metal Dichalcogenides: Applications, Challenges, and Opportunities. *ACS Nano* **2021**, *15*, 2165−2181.

(23) Koós, A. A.; Vancsó, P.; Szendrö, M.; Dobrik, G.; Antognini Silva, D.; Popov, Z. I.; Sorokin, P. B.; Henrard, L.; Hwang, C.; Biró, L. P.; et al. Influence of Native Defects on the Electronic and Magnetic Properties of CVD Grown MoSe₂ Single Layers. *J. Phys. Chem. C* **2019**, *123*, 24855−24864.

(24) Zhou, W.; Dong, L.; Tan, L.; Tang, Q. Understanding the Air Stability of Defective MoS₂ and the Oxidation Effect on the Surface HER Activity. *J. Phys-Condens Mat* **2021**, *33*, 395002.

(25) Lunardon, M.; Kosmala, T.; Ghorbani-Asl, M.; Krasheninnikov, A. V.; Kolekar, S.; Durante, C.; Batzill, M.; Agnoli, S.; Granozzi, G. Catalytic Activity of Defect-Engineered Transition Metal Dichalcogenides Mapped with Atomic-Scale Precision by Electrochemical Scanning Tunneling Microscopy. *ACS Energy Lett.* **2023**, *8*, 972−980.

(26) Feng, Z.; Chen, B.; Qian, S.; Xu, L.; Feng, L.; Yu, Y.; Zhang, R.; Chen, J.; Li, Q.; Li, Q.; et al. Chemical sensing by band modulation of a black phosphorus/molybdenum diselenide van der Waals heterostructure. *2D Mater.* **2016**, *3*, No. 035021.

(27) Yang, Z.; Zhang, D.; Wang, D. Carbon monoxide gas sensing properties of metal-organic frameworks-derived tin dioxide nanoparticles/molybdenum diselenide nanoflowers. *Sensor Actuat B-Chem.* **2020**, *304*, No. 127369.

(28) Zhou, L.; Mi, Q.; Jin, Y.; Li, T.; Zhang, D. Construction of MoO3/MoSe2 nanocomposite-based gas sensor for low detection limit trimethylamine sensing at room temperature. *J. Mater. Sci.: Mater. Electron.* **2021**, *32*, 17301−17310.

(29) Jaiswal, J.; Das, A.; Chetry, V.; Kumar, S.; Chandra, R. NO2 sensors based on crystalline MoSe2 porous nanowall thin films with vertically aligned molecular layers prepared by sputtering. *Sens. Actuator B-Chem.* **2022**, *359*, No. 131552.

(30) Liu, G.; Ahsan, S.; Khitun, A. G.; Lake, R. K.; Balandin, A. A. Graphene-based non-Boolean logic circuits. *J. Appl. Phys.* **2013**, *114*, 154310.

(31) Shu, H.; Zhou, D.; Li, F.; Cao, D.; Chen, X. Defect Engineering in MoSe2 for the Hydrogen Evolution Reaction: From Point Defects to Edges. *ACS Appl. Mater. Interfaces* **2017**, *9*, 42688−42698.

(32) Lee, J.; Kang, S.; Yim, K.; Kim, K. Y.; Jang, H. W.; Kang, Y.; Han, S. Hydrogen Evolution Reaction at Anion Vacancy of Two-Dimensional Transition-Metal Dichalcogenides: Ab Initio Computational Screening. *J. Phys. Chem. Lett.* **2018**, *9*, 2049−2055.

(33) Jain, A.; Sadan, M. B.; Ramasubramaniam, A. Promoting Active Sites for Hydrogen Evolution in MoSe2 via Transition-Metal Doping. *J. Phys. Chem. C* **2020**, *124*, 12324−12336.

(34) Yi, J.; Li, H.; Gong, Y.; She, X.; Song, Y.; Xu, Y.; Deng, J.; Yuan, S.; Xu, H.; Li, H. Phase and interlayer effect of transition metal dichalcogenide cocatalyst toward photocatalytic hydrogen evolution: The case of MoSe2. *Appl. Catal. B: Environ* **2019**, *243*, 330−336.

(35) German, E.; Gebauer, R. Why are MoS2 monolayers not a good catalyst for the oxygen evolution reaction? *Appl. Surf. Sci.* **2020**, *528*, No. 146591.

(36) Karmodak, N.; Andreussi, O. Oxygen Evolution on MoS2 Edges: Activation through Surface Oxidation. *J. Phys. Chem. C* **2021**, *125*, 10397−10405.

(37) Mohanty, B.; Ghorbani-Asl, M.; Kretschmer, S.; Ghosh, A.; Guha, P.; Panda, S. K.; Jena, B.; Krasheninnikov, A. V.; Jena, B. K. MoS2 Quantum Dots as Efficient Catalyst Materials for the Oxygen Evolution Reaction. *ACS Catal.* **2018**, *8*, 1683−1689.

(38) Chan, K.; Tsai, C.; Hansen, H. A.; Nørskov, J. K. Molybdenum Sulfides and Selenides as Possible Electrocatalysts for CO2 Reduction. *ChemCatChem* **2014**, *6*, 1899−1905.

(39) Aguilar, N.; Atilhan, M.; Aparicio, S. Single atom transition metals on MoS2 monolayer and their use as catalysts for CO2 activation. *Appl. Surf. Sci.* **2020**, *534*, No. 147611.

(40) Kang, S.; Han, S.; Kang, Y. Unveiling Electrochemical Reaction Pathways of CO2 Reduction to CN Species at S-Vacancies of MoS2. *ChemSusChem* **2019**, *12*, 2671−2678.

(41) Ye, J.; Rao, D.; Yan, X. Regulating the electronic properties of MoSe2 to improve its CO2 electrocatalytic reduction performance via atomic doping. *New J. Chem.* **2021**, *45*, 5350−5356.

(42) Ren, Y.; Sun, X.; Qi, K.; Zhao, Z. Single atom supported on MoS2 as efficient electrocatalysts for the CO2 reduction reaction: A DFT study. *Appl. Surf. Sci.* **2022**, *602*, No. 154211.

(43) Ramzan, M. A.; Favre, R.; Steinmann, S. N.; Le Bahers, T.; Raybaud, P. Electrocatalytic Reduction Mechanisms of CO2 on MoS2 Edges Using Grand-Canonical DFT: From CO2 Adsorption to HCOOH or CO. *J. Phys. Chem. C* **2024**, *128*, 10025−10034.

(44) Zhang, J.; Ling, C.; Zang, W.; Li, X.; Huang, S.; Li, X. L.; Yan, D.; Kou, Z.; Liu, L.; Wang, J.; et al. Boosted electrochemical ammonia synthesis by high-percentage metallic transition metal dichalcogenide quantum dots. *Nanoscale* **2020**, *12*, 10964−10971.

(45) Qu, H.; He, S.; Su, Y.; Zhang, Y.; Su, H. MoSe2: a promising non-noble metal catalyst for direct ethanol synthesis from syngas. *Fuel* **2020**, *281*, No. 118760.

(46) Ma, D.; Tang, Y.; Yang, G.; Zeng, J.; He, C.; Lu, Z. CO catalytic oxidation on iron-embedded monolayer MoS2. *Appl. Surf. Sci.* **2015**, *328*, 71−77.

(47) Zhu, Y.; Zhao, K.; Shi, J.; Ren, X.; Zhao, X.; Shang, Y.; Xue, X.; Guo, H.; Duan, X.; He, H.; et al. Strain Engineering of a Defect-Free, Single-Layer MoS2 Substrate for Highly Efficient Single-Atom Catalysis of CO Oxidation. *ACS Appl. Mater. Interfaces* **2019**, *11*, 32887−32894.

(48) Zhang, X.; Chang, Q.; Yang, Z.; Wang, W. Surface vacancy on PtTe2 for promoting CO oxidation through efficiently activating O2. *J. Phys-Condens. Mater.* **2020**, *32*, No. 025201.

(49) Guo, J.-X.; Wu, S.-Y.; Zhong, S.-Y.; Zhang, G.-J.; Shen, G.-Q.; Yu, X.-Y. Janus WSSe monolayer adsorbed with transition-metal atoms (Fe, Co and Ni): excellent performance for gas sensing and CO catalytic oxidation. *Appl. Surf. Sci.* **2021**, *565*, No. 150558.

(50) Bombín, R.; Alducin, M.; Juaristi, J. I. N. Adsorption and dissociation of diatomic molecules on monolayer 1H−MoSe2. *Phys. Rev. B* **2022**, *105*, No. 035404.

(51) Kresse, G.; Furthmüller, J. Efficient iterative schemes for ab initio total-energy calculations using a plane-wave basis set. *Phys. Rev. B* **1996**, *54*, 11169−11186.

(52) Dion, M.; Rydberg, H.; Schröder, E.; Langreth, D. C.; Lundqvist, B. I. Van der Waals Density Functional for General Geometries. *Phys. Rev. Lett.* **2004**, *92*, No. 246401.

(53) Blöchl, P. E. Projector augmented-wave method. *Phys. Rev. B* **1994**, *50*, 17953−17979.

(54) Kresse, G.; Joubert, D. From ultrasoft pseudopotentials to the projector augmented-wave method. *Phys. Rev. B* **1999**, *59*, 1758−1775.

(55) Monkhorst, H. J.; Pack, J. D. Special points for Brillouin-zone integrations. *Phys. Rev. B* **1976**, *13*, 5188−5192.

(56) Grimme, S.; Antony, J.; Ehrlich, S.; Krieg, H. A consistent and accurate ab initio parametrization of density functional dispersion correction (DFT-D) for the 94 elements H-Pu. *J. Chem. Phys.* **2010**, *132*, 154104.

(57) Nosé, S. A Unified Formulation of the Constant Temperature Molecular Dynamics Methods. *J. Chem. Phys.* **1984**, *81*, 511−519.

(58) Novko, D.; Lončarić, I.; Blanco-Rey, M.; Juaristi, J. I.; Alducin, M. Energy loss and surface temperature effects in ab initio molecular dynamics simulations: N adsorption on Ag(111) as a case study. *Phys. Rev. B* **2017**, *96*, No. 085437.

(59) Groß, A.; Dianat, A. Hydrogen Dissociation Dynamics on Precovered Pd Surfaces: Langmuir is Still Right. *Phys. Rev. Lett.* **2007**, *98*, No. 206107.

(60) Nattino, F.; Díaz, C.; Jackson, B.; Kroes, G.-J. Effect of Surface Motion on the Rotational Quadrupole Alignment Parameter of **D**2 Reacting on Cu(111). *Phys. Rev. Lett.* **2012**, *108*, No. 236104.

(61) Nattino, F.; Ueta, H.; Chadwick, H.; van Reijzen, M. E.; Beck, R. D.; Jackson, B.; van Hemert, M. C.; Kroes, G.-J. Ab Initio Molecular Dynamics Calculations versus Quantum-State-Resolved Experiments on CHD3 + Pt(111): New Insights into a Prototypical Gas Surface Reaction. *J. Phys. Chem. Lett.* **2014**, *5*, 1294−1299.

(62) Kolb, B.; Guo, H. Communication: Energy transfer and reaction dynamics for DCl scattering on Au(111): An ab initio molecular dynamics study. *J. Chem. Phys.* **2016**, *145*, No. 011102.

(63) Zhou, X.; Kolb, B.; Luo, X.; Guo, H.; Jiang, B. Ab Initio Molecular Dynamics Study of Dissociative Chemisorption and Scattering of CO2 on Ni(100): Reactivity, Energy Transfer, Steering Dynamics, and Lattice Effects. *J. Phys. Chem. C* **2017**, *121*, 5594−5602.

(64) Zhou, L.; Jiang, B.; Alducin, M.; Guo, H. Communication: Fingerprints of reaction mechanisms in product distributions: Eley-Rideal-type reactions between D and CD3/Cu(111). *J. Chem. Phys.* **2018**, *149*, No. 031101.

(65) Füchsel, G.; Zhou, X.; Jiang, B.; Juaristi, J. I.; Alducin, M.; Guo, H.; Kroes, G.-J. Reactive and Nonreactive Scattering of HCl from Au(111): An Ab Initio Molecular Dynamics Study. *J. Phys. Chem. C* **2019**, *123*, 2287−2299.

(66) Rivero Santamaría, A.; Alducin, M.; Díez Muiño, R.; Juaristi, J. I. Ab Initio Molecular Dynamics Study of Alignment-Resolved O2 Scattering from Highly Oriented Pyrolytic Graphite. *J. Phys. Chem. C* **2019**, *123*, 31094−31102.

(67) Rivero Santamaría, A.; Ramos, M.; Alducin, M.; Busnengo, H. F.; Díez Muiño, R.; Juaristi, J. I. High-Dimensional Atomistic Neural Network Potential to Study the Alignment-Resolved O2 Scattering

from Highly Oriented Pyrolytic Graphite. *J. Phys. Chem. A* **2021**, *125*, 2588−2600.

(68) Granja-DelRío, A.; Alducin, M.; Naki Juaristi, J. I.; López, M. J.; Alonso, J. A. Absence of spillover of hydrogen adsorbed on small palladium clusters anchored to graphene vacancies. *Appl. Surf. Sci.* **2021**, *559*, No. 149835.

(69) Quattrucci, J. G.; Jackson, B. Quasiclassical study of Eley−Rideal and hot atom reactions of H atoms with Cl adsorbed on a Au(111) surface. *J. Chem. Phys.* **2005**, *122*, No. 074705.

(70) Zhou, L.; Zhou, X.; Alducin, M.; Zhang, L.; Jiang, B.; Guo, H. Ab initio molecular dynamics study of the Eley-Rideal reaction of H + Cl−Au(111) → HCl + Au(111): Impact of energy dissipation to surface phonons and electron-hole pairs. *J. Chem. Phys.* **2018**, *148*, No. 014702.

(71) Chen, J.; Zhou, X.; Jiang, B. Eley Rideal recombination of hydrogen atoms on Cu(111): Quantitative role of electronic excitation in cross sections and product distributions. *J. Chem. Phys.* **2019**, *150*, No. 061101.

(72) Zhu, L.; Hu, C.; Chen, J.; Jiang, B. Investigating the Eley−Rideal recombination of hydrogen atoms on Cu (111) via a high-dimensional neural network potential energy surface. *Phys. Chem. Chem. Phys.* **2023**, *25*, 5479−5488.

(73) Blanco-Rey, M.; Díaz, E.; Bocan, G. A.; Díez Muiño, R.; Alducin, M.; Juaristi, J. I. Efficient N2 Formation on Ag(111) by Eley−Rideal Recombination of Hyperthermal Atoms. *J. Phys. Chem. Lett.* **2013**, *4*, 3704−3709.

(74) Juaristi, J. I.; Díaz, E.; Bocan, G.; Díez Muiño, R.; Alducin, M.; Blanco-Rey, M. Angular distributions and rovibrational excitation of N2 molecules recombined on N-covered Ag(111) by the Eley−Rideal mechanism. *Catal. Today* **2015**, *244*, 115−121.

(75) Quintas-Sánchez, E.; Larrégaray, P.; Crespos, C.; Martin-Gondre, L.; Rubayo-Soneira, J.; Rayez, J. C. Dynamical Reaction Pathways in Eley-Rideal Recombination of Nitrogen from W(100). *J. Chem. Phys.* **2012**, *137*, No. 064709.

(76) Pétuya, R.; Crespos, C.; Quintas-Sánchez, E.; Larrégaray, P. Comparative Theoretical Study of H$_2$ Eley-Rideal Recombination Dynamics on W(100) and W(110). *J. Phys. Chem. C* **2014**, *118*, 11704−11710.

(77) Galparsoro, O.; Juaristi, J. I.; Crespos, C.; Alducin, M.; Larrégaray, P. Stereodynamics of Diatom Formation through Eley−Rideal Abstraction. *J. Phys. Chem. C* **2017**, *121*, 19849−19858.

(78) Wu, Q.; Zhou, L.; Guo, H. Steric Effects in CO Oxidation on Pt(111) by Impinging Oxygen Atoms Lead to an Exclusive Hot Atom Mechanism. *J. Phys. Chem. C* **2019**, *123*, 10509−10516.

(79) Galparsoro, O.; Pétuya, R.; Busnengo, F.; Juaristi, J. I.; Crespos, C.; Alducin, M.; Larregaray, P. Hydrogen abstraction from metal surfaces: when electron−hole pair excitations strongly affect hot-atom recombination. *Phys. Chem. Chem. Phys.* **2016**, *18*, 31378−31383.

(80) Galparsoro, O.; Busnengo, H. F.; Juaristi, J. I.; Crespos, C.; Alducin, M.; Larregaray, P. Communication: Hot-atom abstraction dynamics of hydrogen from tungsten surfaces: The role of surface structure. *J. Chem. Phys.* **2017**, *147*, 121103.

(81) Galparsoro, O.; Busnengo, H. F.; Martinez, A. E.; Juaristi, J. I.; Alducin, M.; Larregaray, P. Energy dissipation to tungsten surfaces upon hot-atom and Eley−Rideal recombination of H$_2$. *Phys. Chem. Chem. Phys.* **2018**, *20*, 21334−21344.